Limnol. Oceanogr., 49(2), 2004, 330–340

In situ pCO_2 and O_2 measurements in a lake during turnover and stratification: Observations and modeling

Matthew M. Baehr and Michael D. DeGrandpre[1]
Department of Chemistry, The University of Montana, Missoula, Montana 59812

Abstract

Sensors for the partial pressure of CO_2 (pCO_2) and dissolved O_2 (DO) were deployed near the surface and bottom of a freshwater lake (Placid Lake, Montana) during the period from ice cover to seasonal stratification. Sources of variability were examined using one-dimensional physical and biogeochemical models. Model predictions for pCO_2 and DO were compared to further constrain model parameters. A number of transient processes were documented that have not been well characterized in previous studies. The models made it possible to link these short-term events to specific forcings. We found that (1) 11 d of the 13-d turnover period occurred under ice through light-driven convective mixing, (2) phytoplankton biomass increased to its highest seasonal level under ice, (3) weak stratification set up immediately after ice-out, causing bottom water pCO_2 and DO to diverge from surface levels, (4) subsequent diel convective mixing brought bottom pCO_2 and DO back toward surface levels, and (5) before stable stratification, vertical entrainment of CO_2-rich water, net production, and air-water exchange drove 100–200 μatm daily changes in pCO_2, but, because of their counterbalancing effects, surface pCO_2 remained $>$1,000 μatm for nearly 1 month after ice-out. Upon stable stratification, net production and air-water exchange overcame pCO_2 gains from mixing and heating and reduced pCO_2 to near atmospheric levels within 20 d. Net production and gas exchange accounted for $\sim$75% and 25%, respectively, of the decrease in surface pCO_2 observed after ice-out. Diel convection was the dominant mixing process both under ice and after ice-out and may be an important underrepresented mechanism for CO_2 and DO exchange between surface and bottom water.

Spring thaw heralds not only a new growing season but also an important transitional period for ice-covered lakes and reservoirs. Physical forcings change dramatically between ice cover and open water, creating large and rapid changes in lake biology and geochemistry. As ice and snow cover diminishes, light penetration can stimulate phytoplankton growth (e.g., Wright 1964) and convective mixing (Bengtsson 1996). Surface water temperatures <4°C continue to warm and sink or, after ice-out, to be mixed by winds to greater depths, which results in an isothermal water column. Nutrients accumulated over winter combined with increased insolation produce the characteristic spring phytoplankton bloom. With further solar heating, the water column becomes thermally stratified, isolating the bottom water from the atmosphere until turnover occurs again, which is usually in the fall for dimictic lakes. The duration and magnitude of ice cover, turnover, and stratification can dramatically influence the concentrations of biogeochemical species both seasonally and interannually (e.g., Cornett and Rigler 1980; Effler and Perkins 1987; Livingstone 1993; Stefan and Fang 1994). Although each stage of the spring transition is relatively short-lived, our understanding of this period has primarily evolved from temporally sparse data sets. Combined biogeochemical and physical time series with subhourly resolution that span the entire spring-to-summer transition could lead to important insights. Comprehensive data sets such as these are exceedingly rare, however, because autonomous biogeochemical sensors have not been available until relatively recently (Dickey 2001).

We have used autonomous partial pressure of CO_2 (pCO_2) and dissolved O_2 (DO) sensors to characterize CO_2 and O_2 dynamics in marine and freshwater ecosystems (DeGrandpre et al. 1997, 1998; Baehr and DeGrandpre 2002). Our general objective has been to understand the processes that control surface pCO_2 and, consequently, air-water CO_2 fluxes in aquatic ecosystems. We found that relatively few studies have focused on the mechanisms that control CO_2 cycling in lakes. Researchers have typically used CO_2 measurements to quantify other processes such as net community metabolism (e.g., Schindler and Fee 1973; Talling 1976; Rich 1979), air-water gas exchange (Anderson et al. 1999), acidification (Kratz et al. 1987), or global atmospheric fluxes (Cole et al. 1994). For the present study, we examined high-temporal-resolution biogeochemical and physical time series from Placid Lake, a seasonally ice-covered lake in western Montana. Our specific objectives were to (1) characterize the short-term and seasonal pCO_2 and DO variability during the spring-to-summer transition, (2) examine the sources of variability using a coupled physical-biogeochemical model, (3) evaluate the importance of short-term processes in controlling seasonal biogeochemical concentrations and distributions, and (4) determine whether mooring-based instrumentation can be used to effectively study carbon cycling in a relatively simple (e.g., one-dimensional [1-D]) lake ecosys-

[1] Corresponding author (mdegrand@selway.umt.edu).

Acknowledgments

We thank Ed Keller (The University of Montana) and Terry Hammar (Woods Hole Oceanographic Institution) for assistance with fieldwork, Jim Price (Woods Hole Oceanographic Institution) for helpful discussions, Richard Taylor (USDA Forest Service) for meteorological data from the Seeley Lake USDA Ranger Station, and two anonymous reviewers for constructive comments. This paper is dedicated to the memory of Richard Juday (1918–2002), son of pioneering limnologist Chancey Juday, who initiated study on Placid Lake in the early 1980s.

This work was funded in part by grants from MONTS-EPSCoR (grant 292144) and NSF-Ocean Sciences (OCE-9814388).

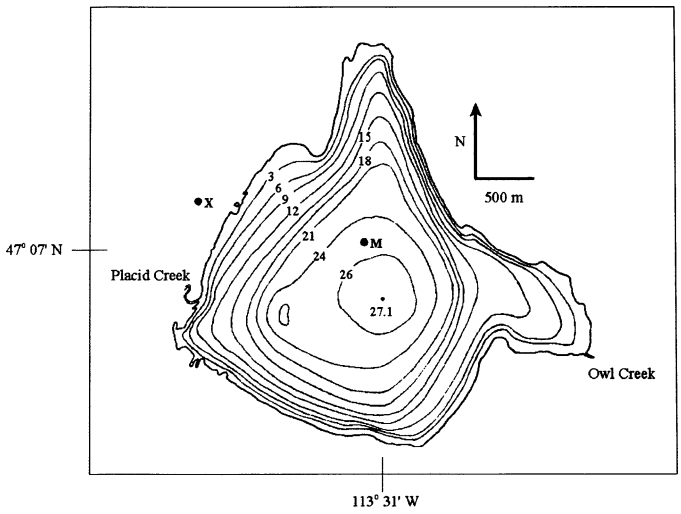

Fig. 1. Bathymetric map of Placid Lake, Montana. M and X designate the locations of the instrumented mooring and meteorological station, respectively. Placid and Owl Creeks are the primary inlet and outlet streams, respectively. Contour intervals are in meters.

tem—if so, these results can be used to guide mooring–based carbon cycle studies in marine ecosystems with more complex hydrography and physical forcings.

Methods

Study site—The study was conducted on Placid Lake (47°07′N, 113°31′W) 45 km northeast of Missoula, Montana (Fig. 1). The dimictic, mesotrophic lake sits in a bowl-shaped basin 1,256 m above sea level (Juday and Keller 1980). The mean and maximum depths are 15 and 27 m, respectively. The surface area is 4.9 km^2. The hydrological residence time of the lake, determined from discharge measurements made on the inlet, Placid Creek, and the outlet, Owl Creek, is ~2 yr (Baehr and DeGrandpre 2002). Groundwater inflow is negligible (Juday and Keller 1980). With the small surface and groundwater inputs, we assumed that the primary sources of variability would arise from within the lake and also that horizontal gradients would be small, making it possible to characterize the lake biogeochemistry with a single vertical array of moored instrumentation.

Autonomous measurements—Overview: A subsurface mooring was deployed near the lake center at 25 m depth from 18 March to 2 July 1999 (Fig. 1). The mooring included in situ sensors for pCO_2, DO, photosynthetically active radiation (PAR), chlorophyll *a* fluorescence, temperature, and depth (Table 1). Instrument arrays were deployed at ~2 and 20 m to obtain time series in the surface and bottom water for interpretation with a two-box model as described below. Additional thermistors were deployed at other depths (Table 1). All instruments were programmed to acquire data every half hour.

Moored pCO_2 measurements: In situ pCO_2 was recorded using the Submersible Autonomous Moored Instrument for CO_2 (SAMI-CO_2) (DeGrandpre et al. 1995). The SAMI-CO_2 was calibrated over the range 200–3,000 μatm by dilution of a 3,000 ppm CO_2 standard with CO_2-free air (DeGrandpre et al. 1995, 1999). An infrared analyzer (LI-COR) calibrated with NIST-traceable CO_2 gas standards was used to verify the pCO_2. Calibrations were performed at 4.0°C, and raw data were corrected for the difference between the in situ and calibration temperature (DeGrandpre et al. 1999). The CO_2 data are reported as wet pCO_2 using the water vapor pressure at the in situ temperature. Measurement precision is estimated to be approximately ± 1 μatm at 300 μatm, ± 12 μatm at 1,400 μatm, and ± 25 μatm at 2,500 μatm. Predeployment accuracy is approximately ± 1 μatm at 360 μatm and is similar to the precision at higher pCO_2 levels. Precision and accuracy are larger at high pCO_2 because of the nonlinear response (DeGrandpre et al. 1999). Accuracy during the deployment was determined by calculating pCO_2 from periodic measurements of dissolved inorganic carbon (DIC) and spectrophotometric pH, as described in Baehr and DeGrandpre (2002) and French et al. (2002). The mean precision of DIC and pH, based on intrasample replicates, were $\pm 0.5\%$ and ± 0.005 pH units, respectively. The precision of the pCO_2 calculated from DIC and pH is estimated to be $\pm 5\%$. The calculated and in situ pCO_2 agreed to within $\pm 8\%$ ($n = 10$) (Fig. 2). No drift was detected within the tolerance of the measurements.

Moored DO measurements: Dissolved O_2 was measured with commercially available autonomous sondes (Model 6000; YSI). Each instrument was calibrated in water-saturated air at 4.0°C. In situ DO accuracy was determined by comparison with periodic Winkler titration of collected samples. Small drift, based on comparison with the Winkler measurements, was corrected by applying a linear offset. The drift-corrected DO sensor measurements agreed with Winkler values to within $\pm 4\%$ ($n = 10$) (Fig. 2).

Table 1. In situ instrumentation deployed under ice on 18 March 1999 and recovered on 02 July 1999. Instrument descriptions are given in the text. The depths are relative to the lake surface on 18 March.

In situ instrument	Parameters measured	Depth (m)
SAMI-CO_2	pCO_2, temperature	2, 20
YSI model 6000	O_2, temperature, depth	2, 20
Chelsea Instruments		
Model Minitracka II	Chl *a* fluorescence	2
LI-COR model LI-192SA	PAR	0.7
Onset Computer model WTA080537	Temperature	0.7, 4.1, 5.1, 6.1, 8.1, 10.1

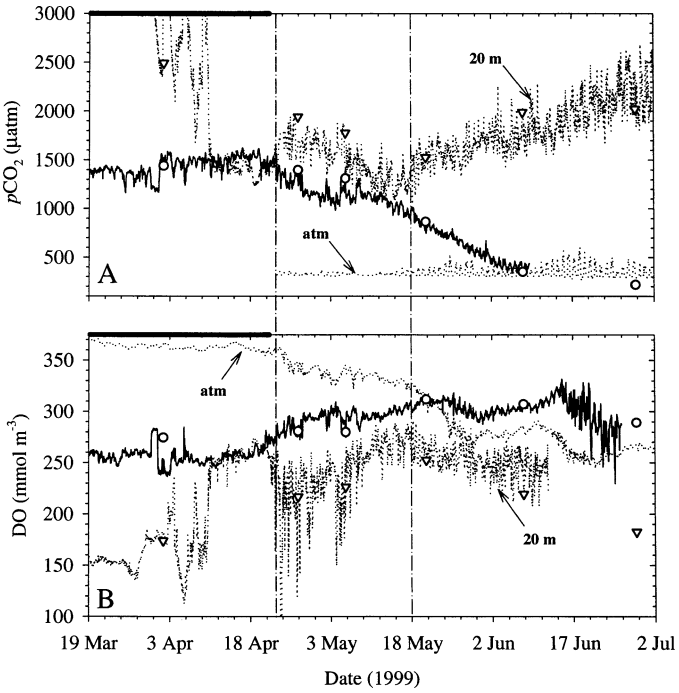

Fig. 2. The 3.5-month in situ time series of (A) pCO_2 and (B) DO at 2 m (black line) and 20 m (dotted and marked **20 m**) and atmospheric saturation (dotted and marked **atm**). Sample measurements at 2 m (open circles) and 20 m (open triangles) used for data quality verification are also shown. Early in the deployment, the 20-m pCO_2 data were beyond the instrument calibration range and are not shown. The DO data shown were corrected for measurement drift (see ''Methods''). The 2-m SAMI and 20-m DO records stopped later in the deployment because of instrument malfunction. Diel fluctuations in atmospheric pCO_2 were caused by an accumulation of terrestrial CO_2 during low wind conditions. Ice cover in this figure and all subsequent figures is indicated by the black bar on the top axis. The two vertical dash-dotted lines bracket the three distinct physical periods discussed in the text: (1) under-ice near isothermal conditions (19 March–23 April), (2) post–ice-out deep mixing (23 April–18 May), and (3) stable stratification (18 May–2 July).

Additional parameters: PAR was measured with a factory-calibrated underwater quantum sensor (Model LI-192SA; LI-COR) attached to the top of the subsurface float (Table 1). Chl *a* fluorescence was measured with an in situ fluorometer (Minitracka II; Chelsea Instruments). The fluorometer was calibrated with samples taken at the depth of the instrument. Chlorophyll was extracted and analyzed with a bench-top spectrofluorometer (Model RF-1501; Shimadzu) (American Public Health Association 1992). The average intersample precision of the method, based on two sample analyses per depth, was ±4%. In situ Chl *a* fluorescence dropped during the day because of fluorescence quenching (e.g., Marra 1997). We therefore linearly interpolated nighttime data from dawn to dusk to obtain daytime values. Profiles of downwelling irradiance were also periodically collected, to determine water attenuation coefficients.

Wind speed and direction and atmospheric pCO_2 were measured every half hour by an autonomous meteorological system stationed in a meadow near the northwest shoreline (Fig. 1). The system included a cup anemometer and wind vane (Model 03001-5; R.M. Young) and an infrared CO_2 analyzer (Model LI-6251; LICOR) powered by a solar panel. Daily high and low air temperature and total daily precipitation were obtained from the USDA Forest Service Seeley Lake Ranger Station, 10 km north of Placid Lake. The air temperature time series was produced by linearly interpolating between the daily high and low temperatures. Barometric pressure and relative humidity were obtained from a NOAA National Data Center site in Missoula, Montana.

Physical model—We used a 1-D mixed-layer model developed for open ocean applications (the PWP model) (Price et al. 1986) to predict mixed-layer depth (MLD) and vertical entrainment (mixing). The MLD was defined as the surface layer where density was homogeneous to within 0.0001 kg m^{-3} (Price et al. 1986). The only significant alteration of the model was the addition of the freshwater equation of state (Chen and Millero 1986). The model requires the input of an initial temperature profile and time-series of heat flux, wind speed, and wind direction. The heat flux includes contributions from net shortwave and longwave radiation, latent heat loss, and sensible heat transfer. The latent heat flux was determined with the evaporation rate of Sill (1983), and the flux of sensible heat was determined with a Bowen convection ratio (e.g., Hostetler and Bartlein 1990). Solar radiation was absorbed within the water column with double-exponential depth dependence (Price et al. 1986). The penetrating shortwave solar radiation was estimated as 40% of the incident solar insolation. Its 1/e attenuation depth was set at 2 m on the basis of periodic downwelling irradiance profiles and Secchi disk depths. Wind stress was calculated as described in Large and Pond (1981). During ice-cover, longwave radiation, latent and sensible heat fluxes, and wind stress were set equal to zero, and only the penetrating portion of the shortwave radiation was input into the model.

Full model—Overview: Coupled physical-biogeochemical lake models range in complexity from simple 1-D descriptions to multilevel food webs with three-dimensional physics (e.g., Riley and Stefan 1988; Van Duin and Lijklema 1989; Karagounis et al. 1993; Stefan and Fang 1994; Jewell 1995; Hamilton and Schladow 1997*a*,*b*). In our case, a simple two-box vertical (1-D) model was the most straightforward to implement and was also well-suited for the two-depth biogeochemical time series. In our two-box model, the surface box, which is also referred to as the surface mixed layer, lies between the air-water interface and the MLD, whereas the bottom box is the water between the MLD and the lake bottom. The thicknesses of the top and bottom boxes are therefore equal to the MLD and 25 m − MLD, respectively.

Separate models were developed for pCO_2 and DO. Because pCO_2 is not a conservative species, mass balances for DIC and total alkalinity (TA) were used, and pCO_2 was calculated from the DIC, TA, and temperature after each time step. The DIC, TA, or DO mass balances are expressed as

$$H\frac{dC}{dt} = F_{\text{GAS}} + F_{\text{NCM}} + F_{\text{ENT}} + F_{\text{ADV}} \qquad (1)$$

where H is either the MLD or bottom box thickness (25 m

− MLD), dC/dt is the rate of change of the chemical species C caused by air-water gas exchange (F_{GAS}), net community metabolism (F_{NCM}) (NCM), vertical entrainment (F_{ENT}), and advection of different water masses (F_{ADV}). Placid Lake was assumed to be horizontally homogeneous ($F_{ADV} = 0$). TA was assumed to be solely carbonate alkalinity and was not affected by gas exchange. Initial TA and DIC values were 1,104 and 1,201 μM, respectively. pCO_2 was calculated using the CO_2 equilibrium constants for zero salinity from Millero (1979) and CO_2 solubility from Weiss (1974). The specific model equations used to quantify each flux term in Eq. 1 are discussed below. Equation parameters were estimated using available data or taken from the literature.

Air-water gas exchange: The air-water flux (F_{GAS}) was calculated using the diffusive boundary layer model:

$$F_{GAS} = K_T S \Delta C \quad (2)$$

where K_T is the gas transfer velocity, S is gas solubility, and ΔC is the partial pressure difference between the atmosphere and surface mixed layer. K_T was estimated using a wind-speed relationship derived from lake tracer studies (eq. 5 in Cole and Caraco 1998) and was adjusted for different temperatures and gases (i.e., DO) using the Schmidt number equations in Wanninkhof (1992). DO gas solubilities were taken from Weiss (1970). Atmospheric partial pressures were calculated from local barometric pressure.

NCM: NCM (F_{NCM}) is the difference between primary production (P) and community respiration (R). P was calculated with a modified exponential model (Platt et al. 1980):

$$P = [\text{Chl } a(P_s\text{Chl}^{-1})(1 - e^{-a})e^{-b}]\theta_P^{(T-3)} \quad (3)$$

where P is in mg C m^{-3} h^{-1} (C is carbon), Chl a the concentration of chlorophyll-a is in mg m^{-3}, P_sChl^{-1} is the assimilation number or Chl a–specific maximum rate of photosynthesis in the absence of photoinhibition (mg C mg Chl a^{-1} h^{-1}), $a = [\alpha Q_{PAR}(P_s\text{Chl}^{-1})]$, α is the Chl a–specific rate of light-limited photosynthesis (mg C mg Chl a^{-1} h^{-1} [μmol quanta m^{-2} s^{-1}]$^{-1}$), Q_{PAR} is the downwelling PAR (μmol quanta m^{-2} s^{-1}), $b = [\beta Q_{PAR}(P_s\text{Chl}^{-1})]$, β is the Chl a–specific photoinhibition parameter (same units as α), θ_P is the Arrhenius temperature coefficient, and T is the in situ temperature in °C.

An α of 0.048 mg C mg Chl a^{-1} h^{-1} (μmol quanta m^{-2} s^{-1})$^{-1}$ was estimated by averaging the rates of change of the 2-m DO data for three different days during the deployment. A β of 0.007 (same units as α) was used because it provided the best overall fit to the dissolved gases. The values for α and β vary greatly in the literature, but our values are not atypical (Platt et al. 1980). An assimilation number (P_sChl^{-1}) of 3.00 mg C mg Chl a^{-1} h^{-1} was used in the model, except for a period when it was decreased to 1.25 (discussed below). These assimilation numbers are within the range reported for other studies (e.g., Prézelin et al. 1991; Fee et al. 1992; Carignan et al. 2000). A temperature coefficient (θ_P) of 1.036 was used (Parkhill and Gulliver 1999). Because the Secchi disk depth was never deeper than 5 m, we assumed that no photosynthesis occurred in the bottom box.

Community respiration (R) was assumed to be only dependent on temperature and was estimated using

$$R = R_3\theta_R^{(T-3)} \quad (4)$$

where R_3 is the respiration rate at 3°C (in mg C m^{-3} h^{-1}) and θ_R is the temperature coefficient. A value of 1.045 was used for R_3 (Parkhill and Gulliver 1999). The surface and bottom R_3 values were 2.40 and 0.36 mg C m^{-3} h^{-1}, respectively. These values are within the range reported for other lakes (e.g., del Giorgio and Peters 1993). The difference in rates between surface and bottom water may have been caused by phytoplankton photorespiration, higher dark respiration in the euphotic zone (Geider 1992), or low sedimentary oxygen demand (Stefan and Fang 1994). We did not explicitly model any of these processes.

The NCM ($P - R$) calculated from Eqs. 3 and 4 was used directly in the DIC (carbon) mass balance. For the DO and TA models, mols of carbon were converted to DO or TA using the Redfield ratios for photosynthetic and respiratory quotients (PQ and RQ)—that is, 138 mol O_2 produced, 106 mol C consumed; 18 mol TA produced, 106 mol C consumed. In the following discussions, NCM > 0 is referred to as net production and NCM < 0 as net respiration.

Vertical entrainment: The MLD output from the PWP model was used with a simple mass balance to quantify the variability arising from vertical entrainment. It was necessary to account for concentration gradients between the surface and bottom water in these calculations. Biogeochemical gradients can extend over a wide depth range because of stagnant conditions in lake bottom water (Wetzel 1983; Babin and Prepas 1985; Livingstone 1993; Stefan and Fang 1994). Our profile samples revealed that gradients often extended from the base of the surface mixed layer to the lake bottom. A linear concentration profile was assumed between the bottom of the surface mixed layer and the lake bottom. When water was entrained into the surface box, the average concentrations of DIC, DO, or TA in the entrained water volume were calculated from the linear gradient. The final dissolved gas concentrations in each box were then calculated by mass balance, taking into account the depth-dependent volume due to the lake bathymetry (Henderson-Sellers and Davies 1989).

Results

Major events and features—Overview: The 3.5-month pCO_2 and DO time series are shown in Fig. 2. Additional data used in the data interpretation and modeling are shown in Fig. 3. Model results are plotted in Figs. 4–6, 8, and 9, and the Chl a profile data are shown in Fig. 7. We first briefly discuss the major features in the physical and biogeochemical time series, broken down into three physically distinct periods: ice cover and turnover, weak stratification and episodic deep mixing, and stable stratification. Sources of variability are then examined using the model described above.

Ice-covered period and turnover (19 March–23 April): The lake was ice covered during the first month of the deployment, as denoted by the black bar on the upper axis of

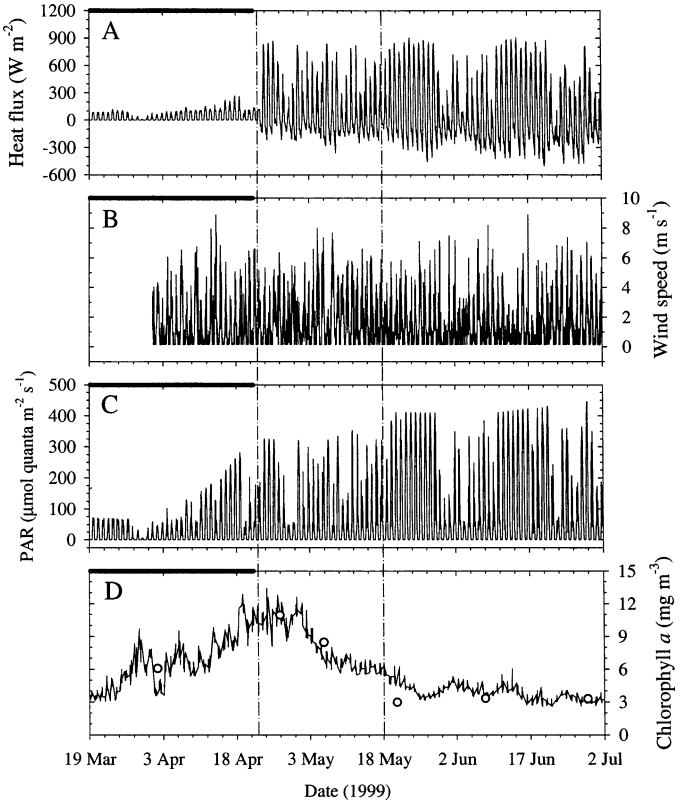

Fig. 3. Supporting data for input into the PWP and biogeochemical models. (A) surface heat flux, (B) wind speed, (C) PAR at 2 m calculated from the 0.7-m PAR record (Table 1) and (D) Chl *a* at 2 m. Periodic profile measurements of Chl *a* are also shown (open circles). The vertical dash-dotted lines are as in Fig. 2.

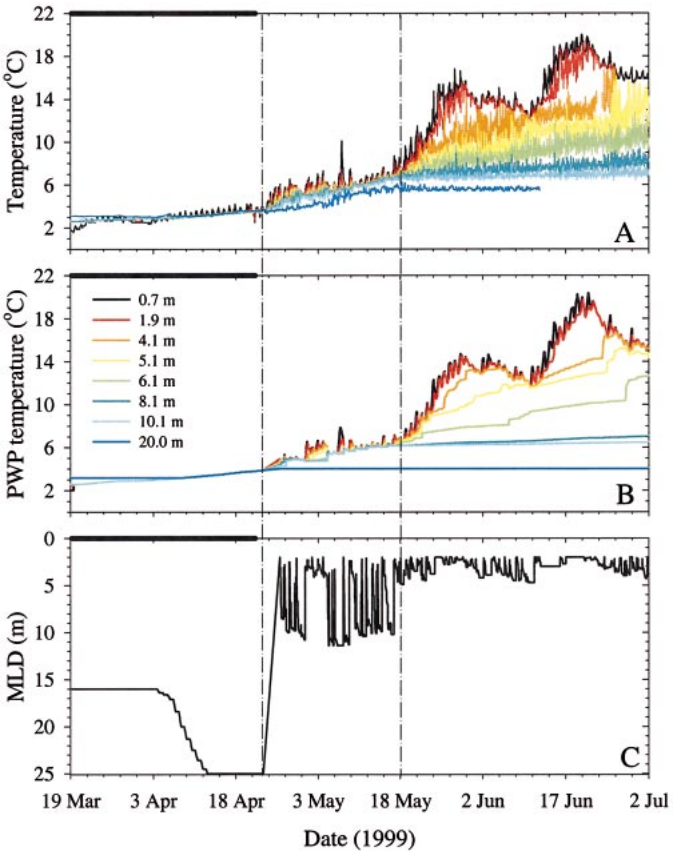

Fig. 4. (A) Measured and (B) PWP modeled temperature time series for depths from 0.7 to 20 m and (C) the predicted MLD. The depths of the in situ and modeled temperature records are given in the color legend on panel B. The vertical dash-dotted lines are as in Fig. 2. The MLD time series shows the three regimes that frame the discussion in the text.

the time-series figures. Large differences in surface and bottom pCO_2 and DO were present at the beginning of the time series (Fig. 2). The pCO_2 and DO were also highly supersaturated and undersaturated, respectively, at both depths. The stratified conditions changed dramatically on ~10 April, when bottom water pCO_2 and DO converged to surface values as a result of complete turnover under ice. On the basis of the temperature time series (Fig. 4A), the water column remained well mixed until 2 d after ice-out (~23 April). The ice-covered period was also marked by significant light penetration and a rapid increase in Chl *a* (Fig. 3C,D). The Chl *a* concentration reached 12 mg m^{-3} at 2 m shortly before ice-out and the maximum in Chl *a* standing stocks also occurred around this time (*see 26 April profile in Fig. 7*).

Weak stratification and episodic deep-mixing (23 April–18 May): This period was distinguished by weak thermal stratification that developed immediately after ice-out (Fig. 4A). The weak stratification isolated the surface from the bottom water, as based on the 2- and 20-m gas concentrations (Fig. 2). Surface and bottom pCO_2 rapidly decreased and increased, respectively, on ~23 April, with opposite trends observed for DO. After ~27 April, the bottom pCO_2 and DO variability reversed direction, slowly decreasing and increasing, respectively, whereas surface gases remained nearly constant (Fig. 2). These trends continued until ~14 May, just before the onset of stable stratification. Meanwhile, Chl *a* remained near peak levels through late April but began a steady decline in early May (Fig. 3D). The progressive increase in PAR was interrupted by extended periods of cloudy weather (Fig. 3C).

Stable stratification (18 May–2 July): On ~18 May, almost a month after ice-out, stable stratification set up and the surface temperature increased rapidly (Fig. 4A). The pCO_2 and DO immediately began to increase and decrease in the bottom water, respectively (Fig. 2). Surface DO increased, becoming supersaturated around 20 May, whereas surface pCO_2 rapidly dropped but remained above atmospheric saturation until ~8 June. A more distinct diel pCO_2 and DO cycle was also observed in the surface data during this period (Figs. 2, 9). Chl *a* dropped to prebloom levels (3–6 mg m^{-3}) in the surface water after 18 May and continued a slow decline until the end of the study (Fig. 3D). Extended periods of cloudy weather were also present (Fig. 3C).

Model and data comparisons: PWP model—Results from the PWP model are shown in Fig. 4B,C. The model repro-

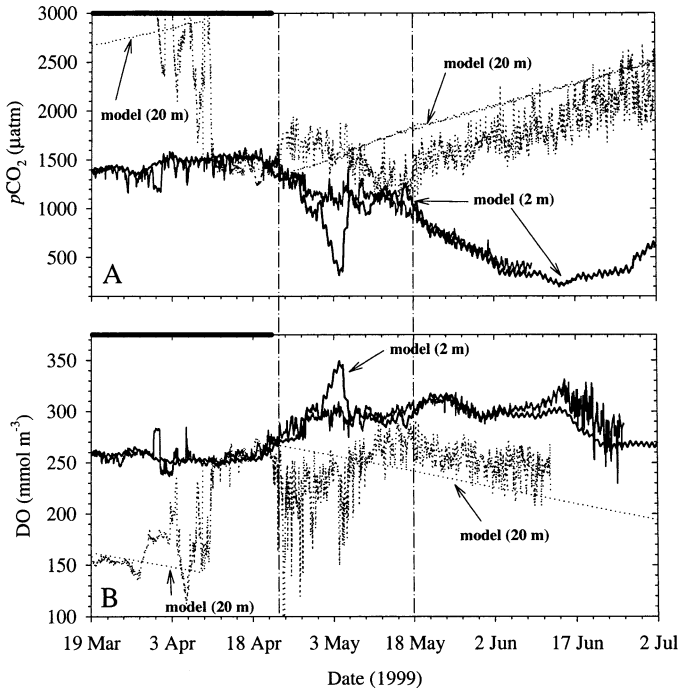

Fig. 5. Biogeochemical model results and time series from Fig. 2 for (A) pCO_2 and (B) DO. Curves are 2 m (black) and 20 m (dotted) for both measured and modeled time series. Model results are marked. See Fig. 2 for atmospheric saturation. The vertical dash-dotted lines are as in Fig. 2.

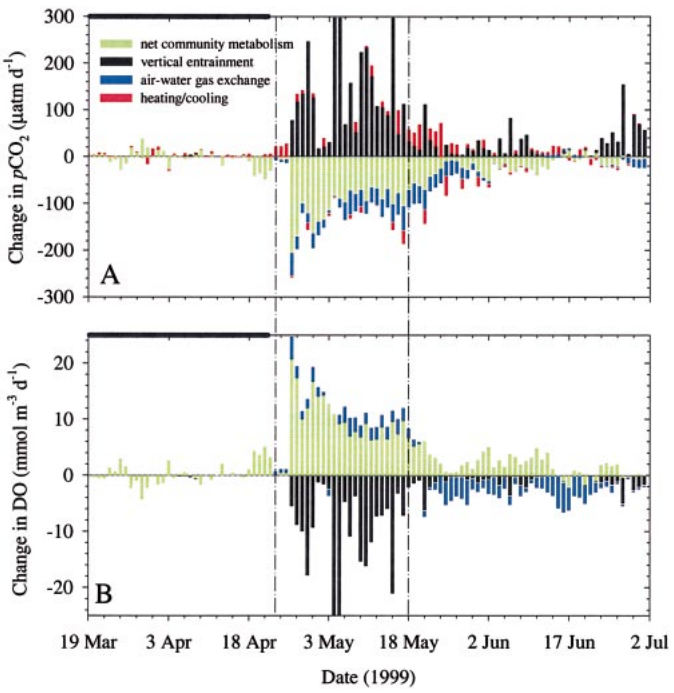

Fig. 6. Modeled daily ± contributions of net community metabolism, vertical entrainment, air-water gas exchange, and heating/cooling to pCO_2 and DO variability in the surface mixed layer calculated from the modeled time series in Fig. 5. In early May, daily pCO_2 and DO changes were >400 μatm and 30 mmol m^{-3}, respectively (off scale), which corresponds to a period when the predicted MLD was too shallow (see text).

duced the major features of the lake thermal structure over the entire 3.5-month period, including the timing of complete turnover (~10 April) and the onset of seasonal stratification (~18 May). The model-derived MLD vividly illustrates the erosion of the surface mixed layer under ice, which, on the basis of the model, began on ~3 April (Fig. 4C). The results of the PWP model indicate that solar radiation transmitted through the ice heated the surface water, which was at <4°C, and the warmer, denser surface water mixed downward. The MLD also revealed a period of deep mixing (23 April–18 May) and a period of more stable stratification when MLDs were <5 m (18 May–2 July) (Fig. 4C). The model did not accurately reproduce the ~2°C temperature increase at 20 m that occurred after ice-out (Fig. 4A). The temperature time series shows that mixing probably extended to this depth (*see the small spikes in the 20-m record around 6 May in Fig. 4A*). We attempted to improve the prediction by varying the Richardson number stability criteria and light attenuation coefficients in the PWP model, but no other combination of parameters fitted the data as well as those used to generate Fig. 4B. Other researchers have found that heat can reach the bottom of the lake through the ''funneling effect'' of the bathymetry (Henderson-Sellers and Davies 1989), and lake mixing models have been developed that consider bathymetry and lake boundaries (e.g., Ivey and Patterson 1984). No lake-specific physical processes were included in the PWP model, but, because the overall prediction was relatively good, it is evident that vertical fluxes of heat and momentum primarily controlled the lake thermal structure.

Model and data comparisons: full model—Overview: The biogeochemical model predictions are compared with the pCO_2 and O_2 time-series in Fig. 5. The long-term magnitude and trends matched the measured time series reasonably well (Fig. 5, Table 2). The model did not accurately predict variability during some periods, as discussed below. We were able to quantify the daily contribution from each process using the model results shown in Fig. 5. The daily changes in pCO_2 and DO are presented in Fig. 6 only for the surface model (for brevity). These figures are discussed as before, first examining the ice-covered period and then the post–ice-out weak and stably stratified periods.

Ice-covered period and turnover (19 March–23 April): On the basis of the modeled contributions in Fig. 6, the major processes at 2 m were NCM and heating/cooling (pCO_2 only). Entrainment was not an important source of variability during the ice-covered period. We were initially confused as to why the surface water gas levels did not change significantly during turnover (10 April, Fig. 5). The model revealed that the entrained water volume, calculated using the bowl-like bathymetry of Placid Lake (Fig. 1), was small relative to the volume of the 15-m MLD at the time of turnover (Fig. 4C). As a consequence, surface-water concentrations remained near preturnover levels. As discussed below, entrainment more dramatically affected surface levels after ice-out.

The model also shows that NCM alternated between extended periods of net production and net respiration under

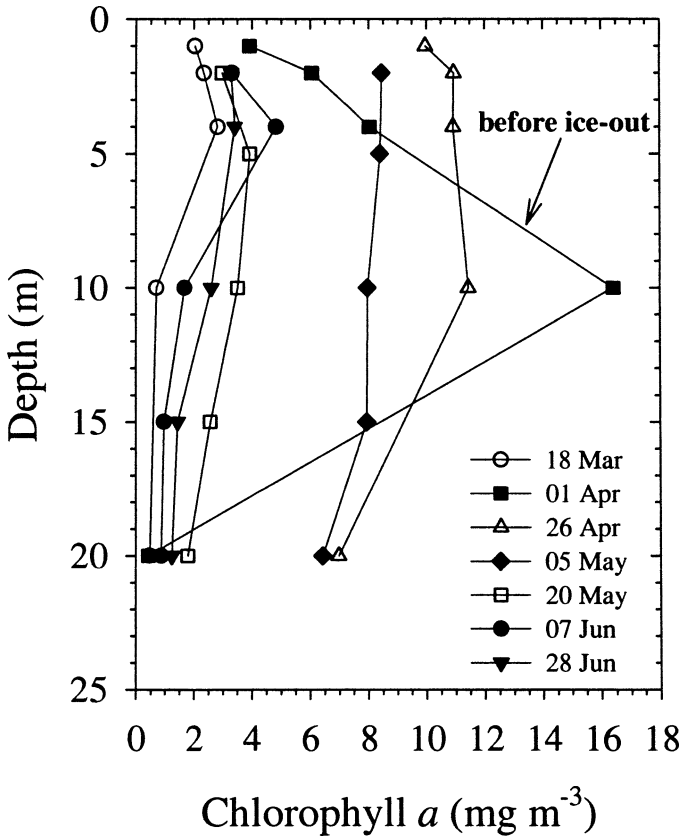

Fig. 7. Chl *a* periodic profile data during the field study. Ice-out occurred between the 1 and 26 April profiles.

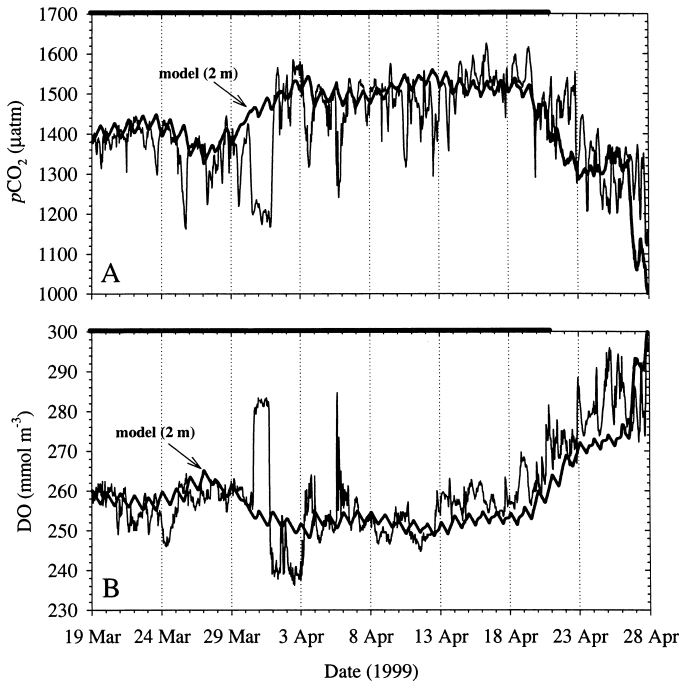

Fig. 8. A 40-d period from Fig. 5 spanning ice cover to ice-out for (A) pCO_2 and (B) DO. Curves are 2 m (black) and model prediction (heavy black and marked). Ice cover is indicated by the black bar on the top axis.

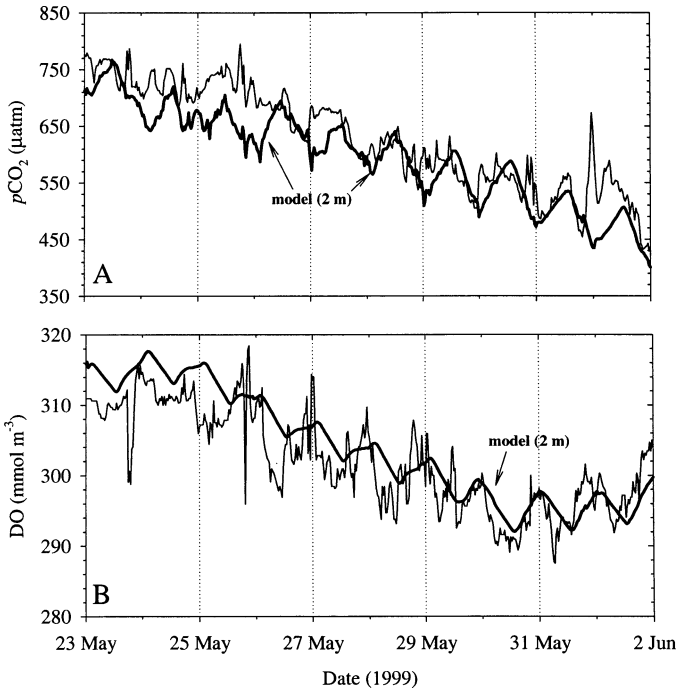

Fig. 9. A 10-d period from Fig. 5 during stable stratification for (A) pCO_2 and (B) DO. Curves are 2 m (black) and model prediction (heavy black and marked).

ice (Fig. 6). Significant changes in light, Chl *a* (Fig. 3C,D), and vertical mixing (Fig. 4C) occurred during this time. Light penetration increased in early April, but Chl *a* dropped (Fig. 3C,D). The drop in Chl *a* coincided with the beginning of vertical entrainment (~3 April, Fig. 4C). The Chl *a* maximum was at ~10 m on 1 April (Fig. 7), which is well below the 1% light level. Chl *a* was also more variable during the under-ice period than after ice-out, when the water column became stratified (Fig. 3D). These observations suggest that light penetration increased phytoplankton standing stocks while also generating convective mixing that moved phytoplankton out of the shallow euphotic zone. Researchers have known for many years that blooms form under ice (e.g.,

Table 2. Model errors from Fig. 5 and sensitivity of the predictions to different parameters. Mean errors were calculated using (modeled-measured)/measured × 100% for each time step (0.5 h).

Parameter	Mean ± SE (%) of pCO_2	Mean ± SE (%) of DO
Model in Fig. 5	−4.3±15	−0.8±4
P_sChl^{-1} = 3.00*	−66.5±43	+22.0±23
P_sChl^{-1} = 1.25*	+89.9±88	−17.6±7
PQ & RQ = 1.0	NA	−2.3±4
PQ & RQ = 2.0	NA	+2.0±5
NCM without temperature	−1.7±14	−1.0±4
No light inhibition†	−30.5±39	+5.8±8
$0.5K_T$	+4.3±17	+0.1±4
$3.0K_T$	−15.6±21	−1.4±6

* Includes under-ice period.
† Jassby and Platt 1976.
NA: not applicable.

Wright 1964; Wetzel 1983) and that under-ice mixing can regulate population growth and species composition (Matthews and Heaney 1987). Our results indicate that these processes also altered NCM and, as a consequence, the pCO_2 and DO levels under ice. The modeled P (Eq. 3) used for other periods was too large during the under-ice convective period (too much CO_2 consumption). To more accurately predict the trends in pCO_2 and DO under ice, we reduced the assimilation number (P_sChl^{-1}) to 1.25 mg C mg Chl a^{-1} h^{-1} from the beginning of convective entrainment (3 April) through ice-out, indirectly accounting for the variable light environment experienced by the mixing phytoplankton. We found that a constant P_sChl^{-1} of 3.00 mg C mg Chl a^{-1} h^{-1} was adequate for all other periods.

Although the overall trends were adequately modeled in the surface water, the observed diel variability differed significantly from the model predictions during the under-ice period (Fig. 8). The modeled diel pCO_2 and DO cycle was primarily driven by the day-night cycle of P and R. The observed pCO_2 and DO often had the opposite phase relationship to the model and, in general, had much larger changes (e.g., 31 March, Fig. 8). Large spikes, down for pCO_2 and up for DO, originated from a relatively constant baseline. Convective mixing could have created short-term variability that was not explained by the model if concentration gradients were present above the sensors (i.e., due to NCM directly under ice or ice-out of solutes) (e.g., Craig et al. 1992). The features were present, however, even after the entire water column became well-mixed (12–23 April, Figs. 4C, 8). We found similar under-ice pCO_2 and DO variability in a previous study of Placid Lake (Baehr and DeGrandpre 2002) and concluded that it was movement of horizontal gradients created by patchiness in the ice and snow cover (Wetzel 1983). Our 1-D model did not include these processes but was able to predict the observed long-term trend (Fig. 8), which suggests that the horizontal gradients had little effect on the mean gas levels at 2 m.

The model also did not predict the large, rapid changes in bottom water pCO_2 and DO before complete turnover on 10 April (Fig. 5). Because these events correspond to periods of increased convective mixing (Fig. 4C), surface water was likely penetrating to this depth. Subsequent mixing with stagnant water below 20 m quickly returned the pCO_2 and DO to earlier levels. Complete turnover on 10 April eliminated the bottom water gradients, and the bottom water remained at surface levels until the onset of weak stratification after ice-out.

Weak stratification and episodic deep mixing (23 April–18 May): The short-term gas variability during the deep-mixing period was not distinctly different from that of other periods (Fig. 5), but the model shows that it was the most dynamic period of the spring transition (Fig. 6). Immediately after ice-out, vertical entrainment was negligible, and net production and gas exchange led to a net pCO_2 draw-down and DO increase (23–27 April, Figs. 6, 8). Surface pCO_2 and DO then leveled off from 1 to 17 May (Fig. 2). The model indicates that net production (NCM $>$ 0) and gas exchange had large daily contributions but that vertical entrainment offset these processes by bringing high CO_2 and low-DO water to the surface (Fig. 6). These large, simultaneous, positive and negative fluxes resulted in relatively constant surface pCO_2 and DO levels. The model deviated significantly from the observations around 1 May, with pCO_2 too low and DO too high (Fig. 5). The deviation appears to have been related to inadequate mixing in the PWP model. The predicted MLD was very shallow (2–4 m) in early May (Fig. 4C), but, on the basis of the in situ temperature records, the MLD was deeper than this and was more variable. Net production and gas exchange rapidly reduced pCO_2 and increased DO in the unrealistically shallow MLD. After 3 May, more mixing was predicted (Fig. 4C), and the gases returned to previous levels as the large volume of subsurface water, which remained near the early May levels using the imposed linear concentration gradient, was mixed with the small surface volume. These results highlight the importance of accurately predicting the magnitude and variability of the MLD.

Although the model was not able to reproduce the variability during all of the deep-mixing period, it is still useful for evaluating the dominant driving forces behind the NCM, vertical mixing, and air-water exchange. The model predicted high rates of net production because of high Chl a and PAR (Fig. 3C,D) and low respiration. Primary production (Eq. 3) averaged ~13 mmol C m^{-3} d^{-1}, compared with an average respiration of ~6 mmol C m^{-3} d^{-1}. Mean net production was therefore ~7 mmol C m^{-3} d^{-1} or ~10 mmol O_2 m^{-3} d^{-1} (*see DO model results in Fig. 6B for molar changes due to NCM*). As discussed above, daily NCM was often counterbalanced by the entrainment of high pCO_2 and low DO subsurface water (Fig. 6). The data in Figs. 3A,B and 4C indicate that nighttime cooling coupled with strong diel winds was the primary forcing for this entrainment. Winds, which typically increased to 4–6 m s^{-1} in the evening (Fig. 3B), efficiently mixed the cooling surface water, creating diel MLD fluctuations ranging from 2–11 m (Fig. 4C). The diel mixing replenished CO_2 in the surface water but also entrained nutrients into the euphotic zone, subsequently fueling net production. Nitrate and phosphate at 2 m (not shown) progressively decreased during this period, which indicates that, eventually, little ''new'' water was entrained by the repetitive diel mixing. Chl a followed a similar decreasing trend (Fig. 3D), which presumably reflects the nutrient depletion.

The diel mixing also reached the bottom water, based on the 20 m pCO_2, DO and temperature time series (Figs. 2, 4A). The pCO_2 and DO, which departed from surface levels shortly after ice-out (23 April), began to go back toward surface levels during the deep-mixing period. pCO_2 and DO continued to decrease and increase, respectively, until strong stratification developed on 18 May. Although, as stated above, the PWP model did not predict mixing to 20 m, the temperature time series suggests that mixing extended to this depth (Fig. 4A). Diel mixing was therefore also an important mechanism for exchange between the surface and bottom water after ice-out. The model underestimated mixing, so the 20 m modeled pCO_2 and DO are too high and too low, respectively (e.g., after 18 May, Fig. 5). Because this process appears to establish bottom-water gas levels prior to more

stable stratification, it is very important to accurately represent diel mixing in lake models.

Stable stratification (18 May–2 July): Surface pCO_2 dropped rapidly after 18 May (Fig. 2), when the water column became stably stratified (Fig. 4C). The model indicates that net production and gas exchange drove this decline, offset somewhat by surface heating and vertical entrainment (Fig. 6). These combined processes drove daily changes in pCO_2 that were often >100 μatm. DO became supersaturated during this period because of net production and heating, which reduced DO saturation (Fig. 2). After ~23 May, daily contributions from individual processes progressively declined (Fig. 6). Net production decreased, even switching to net respiration during brief periods in mid-June. Chl *a* continued to decrease, there were extended cloudy periods (a common characteristic of June in Montana), and respiration increased as surface waters warmed. On sunny days, PAR also became sufficiently high to reduce *P* through light inhibition. Air-water exchange became less important for pCO_2 as it approached atmospheric saturation, but it remained a large source of variability for DO (Fig. 6). Net production and heating sustained DO supersaturation and, consequently, large daily losses from air-water exchange (Figs. 2, 6). Vertical entrainment also continued to be important in the surface but was more episodic, with periods of increased clouds and winds (e.g., early and late June) (Figs. 3, 4C). The episodic entrainment did not appear to reach the bottom water, however. The observed and modeled 20-m pCO_2 and DO levels steadily increased and decreased, respectively, indicating that net respiration was the dominant forcing after stable stratification (Fig. 5). The short-term ''noisy'' variability in the 20-m pCO_2 and DO data presumably originated from the combination of large vertical concentration gradients around the sensors and water movement driven by large scale processes (e.g., internal waves).

After 18 May, distinct diel patterns appeared in the 2 m pCO_2 and DO time series, and the model predicted similar diel amplitudes (Fig. 9). The model's capability to predict the long-term balance of photosynthesis and respiration while also matching the amplitude of the diel cycle was important in constraining the model parameters (Eqs. 3, 4). Much of the shorter term (sub-diel) variability was not modeled accurately. These rapid changes may once again have been due to water movement and gradients within the water column that were not accounted for in the two-box model.

Model sensitivity analysis—We examined the sensitivity of the pCO_2 and DO models to different processes and parameterizations. These results are discussed both quantitatively and qualitatively here, focusing on the surface time series. As presented above, the models were very sensitive to the balance between NCM and vertical entrainment during the deep mixing period. Entrainment not only mixed high pCO_2 and low DO water into the surface but also deepened the mixed layer and thereby dampened the volumetric changes due to air-water exchange. We tested the model sensitivity to mixing and MLD by filtering the MLD time-series to eliminate variability < 3 h, keeping the biological parameters the same. With the reduced mixing frequency, NCM and air-water exchange rapidly decreased and increased pCO_2 and DO, respectively, and both reached atmospheric saturation by mid-May. NCM could have been reduced by changing the parameters for *P* and *R* (Eqs. 3, 4), but no parameters fit the data as well over the entire period, especially after stable stratification on 18 May. We concluded that it was necessary to model these short-term mixing events (<1 h), as shown in the MLD time series (Fig. 4C), to predict the observed variability.

The model was also very sensitive to the parameterization of *P* (*R* was only dependent on temperature). Increasing or decreasing *P* by changing $P_s\text{Chl}^{-1}$ (Eq. 3) dramatically increased the model error (Table 2). The smaller errors for DO reflect its tendency to be held near atmospheric saturation (Fig. 2B) because of its higher rate of air-water exchange. The DO model was somewhat sensitive to the choice of PQ and RQ, mostly because of the change in *P*—for example, a higher PQ increased *P* and overestimated DO (Table 2). The temperature dependence of *P* and *R* essentially cancelled each other—both *P* and *R* increased by about the same amount during the seasonal heating (Table 2). Light inhibition was important over the spring transitional period, however. As discussed earlier, the balance of *P* and *R* occurred around mid-June, when NCM approached zero because of reduced Chl *a* and increased light inhibition (Fig. 6). If a hyperbolic tangent model (Jassby and Platt 1976) was used instead of the light inhibition model, too much production occurred after 18 May, and the model error increased (Table 2). Model results were less sensitive to the parameterization of the gas exchange coefficient (K_T) (Table 2) and, because of the very high pCO_2 supersaturation, pCO_2 predictions were more sensitive to K_T than DO. It should be said that the model is not completely constrained and counterbalancing processes may be simultaneously under or overestimated (e.g., entrainment and NCM as presented above). However, the parameterizations were within reported limits, and the results appear to be reasonable. The pCO_2 and DO model predictions also support that the major sources of variability were accounted for in the model and that mechanisms which might affect one gas and not the other were not important. Calcification, for example, which increases pCO_2 with no change in DO (McConnaughey et al. 1994), was apparently not a significant source of variability.

Discussion

Convective turnover of the water column under ice was one of the more surprising features of the physical and biogeochemical time series. Eleven days of the 13-d turnover period occurred under ice. Light-driven convective mixing under ice has been observed (e.g., Farmer 1975; Matthews and Heaney 1987; Bengtsson 1996), but its effect on biogeochemical distributions has not been well documented. The classical description assumes that complete turnover, with respect to biological and chemical properties, occurs after ice-out (e.g., Wetzel 1983). The conditions for convective mixing under ice have been described by Matthews and Heaney (1987) and include high solar radiation input, a high water extinction coefficient, surface water temperatures

<4°C, and low-density stratification. These conditions exist in many ice-covered temperate lakes; therefore, under-ice convective mixing is probably a common phenomenon and may be an important, underrepresented mechanism for exchange between surface and bottom waters.

Diel deep mixing was also important in establishing the seasonal pCO_2 and DO levels in the lake after ice-out. Model calculations show that, if stable stratification had developed immediately after ice-out on 23 April, the surface gases would have reached atmospheric saturation levels sooner (16 May instead of 1 June for pCO_2 and 4 May instead of 20 May for DO), whereas bottom water DO would have been lower by ~70 mmol m^{-3} by mid-June. Accurate modeling of these processes, including the short-term forcings such as diel winds and convection, is clearly necessary to predict water quality (i.e., DO) in the lake bottom water.

The model revealed that the post–ice-out weakly stratified period was surprisingly dynamic, with large fluxes due to mixing, biological production, and gas exchange. There is evidence that past studies have underestimated the complexity of this period. A number of studies have assumed that changes in CO_2 inventories immediately after ice-out were controlled solely by loss of CO_2 to the atmosphere (Striegl and Michmerhuizen 1998; Anderson et al. 1999; Striegl et al. 2001). Our results indicate that ~900 μatm of the 1,200-μatm decline in pCO_2 observed after ice-out was due to net production (Figs. 5, 6). Many other studies have found high rates of production before and after ice-out (e.g., Wright 1964; Wetzel 1983; Agbeti and Smol 1995). During this time, light and nutrients are plentiful, whereas low temperatures inhibit grazing and microbial respiration. These conditions can create rapid increases in photosynthetic biomass early in the spring, as we observed. The use of CO_2 inventories for predicting air-water gas exchange rates may therefore derive erroneously high rates if the biological uptake of CO_2 is not quantified.

The in situ biogeochemical sensors deployed in Placid Lake, Montana, captured important transient events that, when coupled with model interpretation, revealed the dynamic nature of the spring transition. We observed convective turnover under ice, an under-ice bloom of phytoplankton that equaled the maximum in seasonal biomass, weak stratification immediately after ice-out that isolated the bottom water from the surface, diel mixing of subsurface CO_2-rich water that offset CO_2 losses from net production and gas exchange, and the rapid onset of stable stratification. These transient physical and biological processes significantly altered biogeochemical concentrations and distributions within the water column and demonstrate the importance of quantifying short-term (e.g., diel) forcings in lakes. Our results also support that long-term high-temporal-resolution time series can be used to develop a quantitative understanding of complex aquatic ecosystems (e.g., the coastal oceans). Future mooring-based studies should endeavor to understand relationships among the food web, nutrient dynamics, and pCO_2—for example, what controlled the phytoplankton biomass shown in Fig. 3D? This goal may be accomplished in the future by combining pCO_2 and DO sensors with bio-optical sensors and in situ sampling methods (e.g., continuous plankton recorders sediment traps).

References

AGBETI, M. D., AND J. P. SMOL. 1995. Winter limnology: A comparison of physical, chemical and biological characteristics in two temperate lakes during ice cover. Hydrobiologia **304:** 221–234.

AMERICAN PUBLIC HEALTH ASSOCIATION. 1992. Standard methods for the examination of water and wastewater, 18th ed. American Public Health Association.

ANDERSON, D. E., R. G. STRIEGL, D. I. STANNARD, C. M. MICHMERHUIZEN, T. A. MCCONNAUGHEY, AND J. W. LABAUGH. 1999. Estimating lake-atmosphere CO_2 exchange. Limnol. Oceanogr. **44:** 988–1001.

BABIN, J., AND E. E. PREPAS. 1985. Modelling winter oxygen depletion rates in ice-covered temperate zone lakes in Canada. Can. J. Fish. Aquat. Sci. **42:** 239–249.

BAEHR, M. M., AND M. D. DEGRANDPRE. 2002. Under-ice CO_2 and O_2 variability in a freshwater lake. Biogeochemistry **61:** 95–113.

BENGTSSON, L. 1996. Mixing in ice-covered lakes. Hydrobiologia **322:** 91–97.

CARIGNAN, R., D. PLANAS, AND C. VIS. 2000. Planktonic production and respiration in oligotrophic Shield lakes. Limnol. Oceanogr. **45:** 189–199.

CHEN, C. A., AND F. J. MILLERO. 1986. Precise thermodynamic properties for natural waters covering only the limnological range. Limnol. Oceanogr. **31:** 657–662.

COLE, J. J., AND N. F. CARACO. 1998. Atmospheric exchange of carbon dioxide in a low-wind oligotrophic lake measured by the addition of SF_6. Limnol. Oceanogr. **43:** 647–656.

———, ———, G. W. KLING, AND T. K. KRATZ. 1994. Carbon dioxide supersaturation in the surface waters of lakes. Science **265:** 1568–1570.

CORNETT, R. J., AND F. H. RIGLER. 1980. The areal hypolimnetic oxygen deficit: An empirical test of a model. Limnol. Oceanogr. **25:** 672–679.

CRAIG, H., R. A. WHARTON, AND C. P. MCKAY. 1992. Oxygen supersaturation in ice-covered Antarctic lakes: Biological versus physical contributions. Science **255:** 318–321.

DEGRANDPRE, M. D., M. M. BAEHR, AND T. R. HAMMAR. 1999. Calibration-free optical chemical sensors. Anal. Chem. **71:** 1152–1159.

———, T. R. HAMMAR, S. P. SMITH, AND F. L. SAYLES. 1995. In situ measurements of seawater pCO_2. Limnol. Oceanogr. **40:** 969–975.

———, ———, D. W. R. WALLACE, AND C. D. WIRICK. 1997. Simultaneous mooring-based measurements of seawater CO_2 and O_2 off Cape Hatteras, North Carolina. Limnol. Oceanogr. **42:** 21–28.

———, ———, AND C. D. WIRICK. 1998. Short-term pCO_2 and O_2 dynamics in California coastal waters. Deep-Sea Res. II **45:** 1557–1575.

DEL GIORGIO, P. A., AND R. H. PETERS. 1993. Balance between phytoplankton production and plankton respiration in lakes. Can. J. Fish. Aquat. Sci. **50:** 282–289.

DICKEY, T. D. 2001. The role of new technology in advancing ocean biogeochemical research. Oceanography **14:** 108–120.

EFFLER, S. W., AND M. G. PERKINS. 1987. Failure of spring turnover in Onondaga lake, NY, U.S.A. Water Air Soil Pollut. **34:** 285–291.

FARMER, D. M. 1975. Penetrative convection in the absence of mean shear. Q. J. R. Meteorol. Soc. **101:** 869–891.

FEE, E. J., J. A. SHEARER, E. R. DEBRUYN, AND E. U. SCHINDLER. 1992. Effects of lake size on phytoplankton photosynthesis. Can. J. Fish. Aquat. Sci. **49:** 2445–2459.

FRENCH, C. R., J. J. CARR, E. M. DOUGHERTY, L. A. K. EIDSON, J.

C. REYNOLDS, AND M. D. DEGRANDPRE. 2002. Spectrophotometric measurements of freshwater pH. Anal. Chim. Acta **453:** 13–20.

GEIDER, R. J. 1992. Respiration: Taxation without representation? p. 333–360 *In* P. G. Falkowski and A. D. Woodhead [eds.], Primary productivity and biogeochemical cycles in the sea. Plenum.

HAMILTON, D. P., AND S. G. SCHLADOW. 1997*a*. Prediction of water quality in lakes and reservoirs. Part I: Model description. Ecol. Model. **96:** 91–110.

———, AND S. G. SCHLADOW. 1997*b*. Prediction of water quality in lakes and reservoirs. Part II: Model calibration, sensitivity analysis and application. Ecol. Model. **96:** 111–123.

HENDERSON-SELLERS, B., AND A. M. DAVIES. 1989. Thermal stratification modeling for oceans and lakes, p. 86–156. *In* C. L. Tien and T. C. Chawla [eds.], Annual review of numerical fluid mechanics and heat transfer, Vol. II. Hemisphere Publ. Corp.

HOSTETLER, S. W., AND P. J. BARTLEIN. 1990. Simulation of lake evaporation with application to modeling lake level variations of Harney-Malheur Lake, Oregon. Water Resour. Res. **26:** 2603–2612.

IVEY, G. N., AND J. C. PATTERSON. 1984. A model of the vertical mixing in Lake Erie in summer. Limnol. Oceanogr. **29:** 553–563.

JASSBY, A. D., AND T. PLATT. 1976. Mathematical formulation of the relationship between photosynthesis and light for phytoplankton. Limnol. Oceanogr. **21:** 540–547.

JEWELL, P. W. 1995. A simple surface water biogeochemical model. 1. Description, sensitivity analyses, and idealized simulations. Water Resour. Res. **31:** 2047–2057.

JUDAY, R. E., AND E. J. KELLER. 1980. A water quality study of Placid Lake and its drainages. MWRRC report 110. Montana State Univ.

KARAGOUNIS, I., J. TROSCH, AND F. ZAMBONI. 1993. A coupled physical-biochemical lake model for forecasting water quality. Aquat. Sci. **55:** 87–102.

KRATZ, T. K., R. B. COOK, C. J. BOWSER, AND P. L. BREZONIK. 1987. Winter and spring pH depressions in northern Wisconsin lakes caused by increases in pCO_2. Can. J. Fish. Aquat. Sci. **44:** 1082–1088.

LARGE, W. G., AND S. POND. 1981. Open ocean momentum flux measurements in moderate to strong winds. J. Phys. Oceanogr. **11:** 324–336.

LIVINGSTONE, D. M. 1993. Lake oxygenation: Application of a one-box model with ice cover. Int. Rev. Ges. Hydrobiol. **78:** 465–480.

MARRA, J. 1997. Analysis of diel variability in chlorophyll fluorescence. J. Mar. Res. **55:** 767–784.

MATTHEWS, P. C., AND S. I. HEANEY. 1987. Solar heating and its influence on mixing in ice-covered lakes. Freshw. Biol. **18:** 135–149.

MCCONNAUGHEY, T. A., J. W. LABAUGH, D. O. ROSENBERRY, R. G. STRIEGL, M. M. REDDY, P. F. SCHUSTER, AND V. CARTER. 1994. Carbon budget for a groundwater-fed lake: Calcification supports summer photosynthesis. Limnol. Oceanogr. **39:** 1319–1332.

MILLERO, F. J. 1979. The thermodynamics of the carbonate system in seawater. Geochim. Cosmochim. Acta **43:** 1651–1661.

PARKHILL, K. L., AND J. S. GULLIVER. 1999. Modeling the effect of light on whole-stream respiration. Ecol. Model. **117:** 333–342.

PLATT, T., C. L. GALLEGOS, AND W. G. HARRISON. 1980. Photoinhibition of photosynthesis in natural assemblages of marine phytoplankton. J. Mar. Res. **38:** 687–701.

PRÉZELIN, B. B., M. M. TILZER, O. SCHOFIELD, AND C. HAESE. 1991. The control of the production process of phytoplankton by the physical structure of the aquatic environment with special reference to its optical properties. Aquat. Sci. **53:** 136–186.

PRICE, J. F., R. A. WELLER, AND R. PINKEL. 1986. Diurnal cycling: Observations and models of the upper ocean response to diurnal heating, cooling, and wind mixing. J. Geophys. Res. **91:** 8411–8427.

RICH, P. H. 1979. Differential CO_2 and O_2 benthic community metabolism in a soft-water lake. J. Fish. Res. Bd. Can. **36:** 1377–1389.

RILEY, M. J., AND H. G. STEFAN. 1988. MINLAKE: A dynamic lake water quality simulation model. Ecol. Model. **43:** 155–182.

SCHINDLER, D. W., AND E. J. FEE. 1973. Diurnal variation of dissolved inorganic carbon and its use in estimating primary production and CO_2 invasion in lake 227. J. Fish. Res. Bd. Can. **30:** 1501–1510.

SILL, B. L. 1983. Free and forced convection effects on evaporation. J. Hydraul. Engin. ASCE **109:** 1216–1231.

STEFAN, H. G., AND X. FANG. 1994. Dissolved oxygen model for regional lake analysis. Ecol. Model. **71:** 37–68.

STRIEGL, R. G., P. KORTELAINEN, J. P. CHANTON, K. P. WICKLAND, G. C. BUGNA, AND M. RANTAKARI. 2001. Carbon dioxide partial pressure and ^{13}C content of north temperate and boreal lakes at spring ice melt. Limnol. Oceanogr. **46:** 941–945.

———, AND C. M. MICHMERHUIZEN. 1998. Hydrologic influence on methane and carbon dioxide dynamics at two north-central Minnesota lakes. Limnol. Oceanogr. **43:** 1519–1529.

TALLING, J. F. 1976. The depletion of carbon dioxide from lake water by phytoplankton. J. Ecol. **64:** 79–121.

VAN DUIN, E. H. S., AND L. LIJKLEMA. 1989. Modelling photosynthesis and oxygen in a shallow, hypertrophic lake. Ecol. Model. **45:** 243–260.

WANNINKHOF, R. 1992. Relationship between wind speed and gas exchange over the ocean. J. Geophys. Res. **97:** 7373–7382.

WEISS, R. F. 1970. The solubility of nitrogen, oxygen and argon in water and seawater. Deep-Sea Res. **17:** 721–735.

———. 1974. Carbon dioxide in water and seawater: The solubility of a non-ideal gas. Mar. Chem. **2:** 203–215.

WETZEL, R. G. 1983. Limnology, 2nd ed. Saunders.

WRIGHT, R. T. 1964. Dynamics of a phytoplankton community in an ice-covered lake. Limnol. Oceanogr. **9:** 163–178.

Received: 7 March 2003
Accepted: 5 November 2003
Amended: 27 November 2003